Simulation of Two-Dimensional Gravity-Driven Unstable Flow

R. Z. Dautov [a], A. G. Egorov [a], J. L. Nieber [b] and A. Y. Sheshukov [b] *

[a]Kazan State University, Kremlyovskaya 18, Kazan, 420008, Russia

[b]University of Minnesota, 1390 Eckles Avenue, Saint Paul, MN 55108, U.S.A.

The coupled equations for flow in unsaturated soil as proposed by Beliaev and Hassanizadeh [6] are described. These equations account for mechanism of dynamic capillary pressure via a first order relaxation function. A form of the relaxation function for the dynamic capillary pressure-saturation relation is proposed based on physical reasoning and a semi-analytical solution to the flow equations. A mass conservative and computational efficient numerical solution to the coupled equations in two space dimensions is derived and applied to the simulation of gravity-driven unstable flow. Simulated fingers have all the morphological features of fingers observed in laboratory experiments. The results demonstrate that the dynamic capillary pressure mechanism causes initial destabilization of the flow, while the mechanism of capillary hysteresis leads to finger persistence.

1. Introduction

There are two main requirements for modeling the phenomenon of gravity-driven fingering in unsaturated porous media: (i) the mathematical model must be capable of producing unstable perturbations, and (ii) the growing perturbations have to be persistent. In our previous work [1] a linear stability analysis was applied to the basic traveling wave solution, and we studied the conditions for the growth of perturbations. We analyzed three distinct models: (i) the conventional Richards equation (RE), (ii) a sharp front Richards equation (SFRE) [2], and (iii) an extended Richards equation with a non-equilibrium pressure-saturation function (RRE) [3]. The analysis by Egorov et al. [1] shows that among the three models considered the RRE model is the only model capable of generating a structured field of fingers from a slightly perturbed uniform wetting flow.

It was shown in [4, 5] that persistence of fingers is dominated by hysteresis in the capillary pressure-saturation relation. Therefore, the hysteresis must be incorporated in the model. Beliaev and Hassanizadeh [6] recently extended the RRE model to what we refer to as the HRRE model, by accounting for hysteresis. In this paper we formulate the HRRE model, develop a numerical solution scheme, and then apply it to two-dimensional simulation of finger propagation. Two cases are considered, the case of a single finger

*The authors wish to acknowledge support under NATO Collaborative Linkage Grant 978242. This work was supported in part by the Army High Performance Computing Research Center under the auspices of the Department of the Army, Army Research Laboratory cooperative agreement number DAAD19-01-2-0014, the content of which does not necessarily reflect the position or the policy of the government, and no official endorsement should be inferred.

generated from a finite surface source, and the case of multiple fingers generated from a slightly perturbed initially uniform field.

2. Problem formulation

Unsaturated flow in porous media is usually modeled using the Richards equation. This equation may be written in dimensionless form as

$$\frac{\partial s}{\partial t} - \nabla \cdot K(s)\nabla p + \frac{\partial}{\partial z} K(s) = 0 \tag{1}$$

$$p = P(s) \tag{2}$$

where s is the effective saturation ($0 \leq s \leq 1$), p is the water pressure, K is the relative hydraulic conductivity, $P(s)$ is the equilibrium pressure represented by the capillary pressure-saturation relationship, and z is the vertical coordinate taken positive downward. Note that in general $P(s)$ can be hysteretic. The HRRE model, like the RRE model, represents the extension of the RE model to incorporate the mechanism of relaxation in the relation between capillary pressure and water saturation. The mechanism of relaxation or dynamic memory effects has been evidenced in numerous experimental reports [7, 8, 9]. The extension of the RE model does not change (1), but replaces the relationship (2).

The HRRE model deals with hysteresis, and, therefore, two main hysteretic curves: $p = P_w(s)$ (main wetting curve or MWC) and $p = P_d(s)$ (main drainage curve or MDC), are incorporated in the model. These two curves divide the (p, s)-plane into three domains: the main hysteretic loop H_0, the domain H_w above the MWC, and the domain H_d below the MDC (Figure 1). The HRRE model postulates [6] that dynamic memory effects (relaxation) are significant only outside the main hysteretic loop, and it takes those effects into account using the same modification of the capillary pressure-saturation relation as in the RRE model [3]

$$\tau_i \frac{\partial s}{\partial t} \equiv \tau_i \dot{s} = p - P_i(s), \qquad (p, s) \in H_i, \quad i = w, d \tag{3}$$

where $\tau_i > 0$ denotes the relaxation coefficient function. As a result of this postulate it is assumed that inside the main hysteretic loop region H_0, wetting/drainage processes follow equilibrium scanning curves. In this paper we use the hysteresis model of Mualem [10] in contrast to the play-type hysteresis model used in [6], and restrict our attention only to the two-stage wetting-drainage process. Trajectories for the wetting stage locate within H_w, while trajectories for the drainage stage will be limited to H_0. The non-equilibrium drainage domain H_d will never be visited for this two-stage process. As a result of the applied conditions scanning curves turn out to be the primary drainage scanning curves [10], yielding the relations

$$p = P_{sc}(s, s_*) \qquad \text{or} \qquad s = S_{sc}(p, s_*) \qquad \text{for} \quad (p, s) \in H_0 \tag{4}$$

$$S_{sc}(p, s_*) = S_w(p) + \frac{s_* - S_w(p)}{1 - S_w(p)} \left(S_d(p) - S_w(p)\right) \tag{5}$$

where S_{sc}, S_w, and S_d are the inverse functions of P_{sc}, P_w, and P_d respectively, and s_* corresponds to the switching point (point 2 in Figure 1). Equations (3) and (4) may

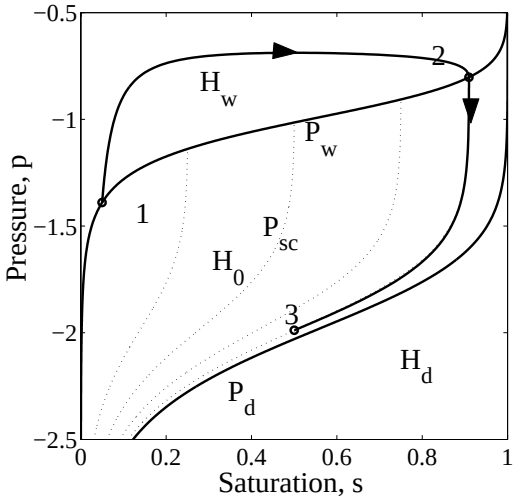

Figure 1. A typical closed-loop hysteresis diagram. The dash line represents the scanning drainage curve. The trajectory of the process follow points 1 (initial state), 2 (switching point), and 3 (final state).

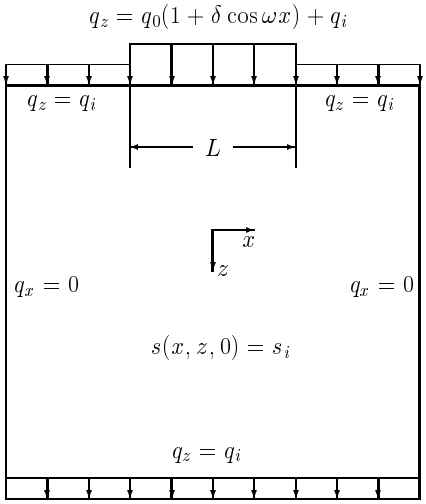

Figure 2. Schematic of the computational domain with specified initial and boundary conditions ($\vec{q} = -K\nabla(p - z)$ and $q_i = -K(s_i)$).

be transformed to one equation by the following. We introduce a set Σ of continuously differentiable functions having a unique maximum and no minimums in $(0, \infty)$. For any $t > 0$ we define the non-local Volterra-type operator $P_t(\cdot) : \Sigma \to \Sigma$ and the inverse operator $S_t(\cdot)$ so that, if $p = P_t(s)$ then $s = S_t(p)$:

$$P_t(s) = \begin{cases} P_w(s(t)), & \dot{s} \geq 0, \\ P_{sc}(s(t), s_*), & \dot{s} < 0 \end{cases}, \qquad S_t(p) = \begin{cases} S_w(p(t)), & \dot{p} \geq 0, \\ S_{sc}(p(t), p_*), & \dot{p} < 0 \end{cases}$$

where $s_* = \max s(t)$, and $p_* = P_w(s_*)$. Then, the capillary pressure-saturation relations (3) and (4) may be rewritten in terms of P_t as

$$\tau\dot{s} = p - P_t(s), \qquad \tau = \begin{cases} \tau_w, & (p, s) \in H_w, \\ 0, & (p, s) \in H_0. \end{cases} \tag{6}$$

To specify the HRRE model, it is necessary to define the hydraulic properties of the medium such as K, P_w and P_d, as well as τ_w as a function of parameters of the process. In this paper we use the Van Genuchten-Mualem model [11] and specify the dimensionless inverse capillary length as $\alpha_w = 1$ and $\alpha_d = 0.5$, and pore size distribution parameter $n_w = n_d = 10$. These parameters correspond to coarse sandy soils, the texture usually used to observe fingering in laboratory experiments.

The functional form for τ_w has not been reliably established previously, but to model finger flow it is essential to establish a robust functional form. A brief description of an analysis to establish such a functional form will now be given. This analysis is based on

the traveling wave solution of the HRRE model. This solution may be derived analogously to that for the RRE model [1]. The analysis shows that τ_w being a function only of s postulated in [3, 6] leads to non-physical behavior of the traveling wave solution for small initial saturation s_i. The trajectory of the wetting process is shown in the (p, s)-plane in Figure 3a. It is observed that $p \to +\infty$ as $s_i \downarrow 0$, a non-physical condition for porous media. This non-physical behavior may be corrected if we assume that τ_w also depends on p, for example:

$$\tau_w = \tau_s(s)\,(p_0 - p)_+^{\gamma}\,, \qquad \gamma > 0$$

where $(\cdot)_+ = \max(\cdot, 0)$, and p_0 is the parameter referred to as the water entry pressure of the soil [2, 12]. For the function τ_w specified above, there is the limiting trajectory as $s_i \downarrow 0$ (Figure 3b), and it corresponds to the sharp-front traveling wave solution, SFRE [1]. It is precisely this behavior that was observed in experiments on initially dry coarse porous media by Selker et al. [2].

From the physical standpoint, one may reason that $\tau_s(s)$ grows to infinity as s approaches either zero, or unity [13]. In two-dimensional calculations we tested various functions $\tau_s(s)$ with power singularities at the ends of the interval $(0, 1)$. The solution was found to be qualitatively the same for all of the calculations. Therefore, in this paper we present results only for $\tau_s(s) = \tau_s^0 P_w'(s)$ which yields the capillary pressure-saturation relation as

$$\tau(p, s)\dot{P}_t(s) = p - P_t(s) \tag{7}$$

where $\tau(p, s) = \tau^0 \cdot (p_0 - p)_+^{\gamma}$, and τ^0 coincides with τ_s^0 inside H_w and holds to zero inside H_0. In the actual calculations, rather than setting $\tau^0 = 0$ inside H_0, it is set to a small constant $\simeq 10^{-3}$. Using this small value serves to allow the description of processes inside and outside the main hysteretic loop by the same procedure, thus facilitating the use of the same algorithm in all computations.

3. Discretization and solution of the HRRE

To numerically solve the system of equations (1) and (7) with initial and boundary conditions shown in Figure 2, we use a mass-conservative approximation and evaluate the temporal terms using a fully implicit first-order backward Euler scheme. To approximate the spatial derivatives we use a finite-difference method with uniform mesh in the z-direction with grid-size h_z and non-uniform mesh in the x-direction with grid-sizes $h_{x,i}$. As a result we have the following algebraic equations in the internal grid points on arbitrary time level $t = t^n$:

$$\begin{aligned}\frac{s_{i,j} - \check{s}_{i,j}}{\Delta t} + \frac{1}{\hbar_{x,i}}\left(k_{i-1/2,j}(s)\frac{H_{i,j} - H_{i-1,j}}{h_{x,i-1}} + k_{i+1/2,j}(s)\frac{H_{i,j} - H_{i+1,j}}{h_{x,i}}\right) \\ + \frac{1}{h_z^2}\left(k_{i,j-1/2}(s)\,(H_{i,j} - H_{i,j-1}) + k_{i,j+1/2}(s)\,(H_{i,j} - H_{i,j+1})\right) = 0\end{aligned} \tag{8}$$

$$\tau(p_{i,j}, s_{i,j})\frac{\Pi_{i,j} - \check{\Pi}_{i,j}}{\Delta t} = p_{i,j} - \Pi_{i,j}, \qquad s_{i,j} = S_t(\Pi_{i,j}), \qquad p_{i,j} = H_{i,j} + Z_{i,j} \tag{9}$$

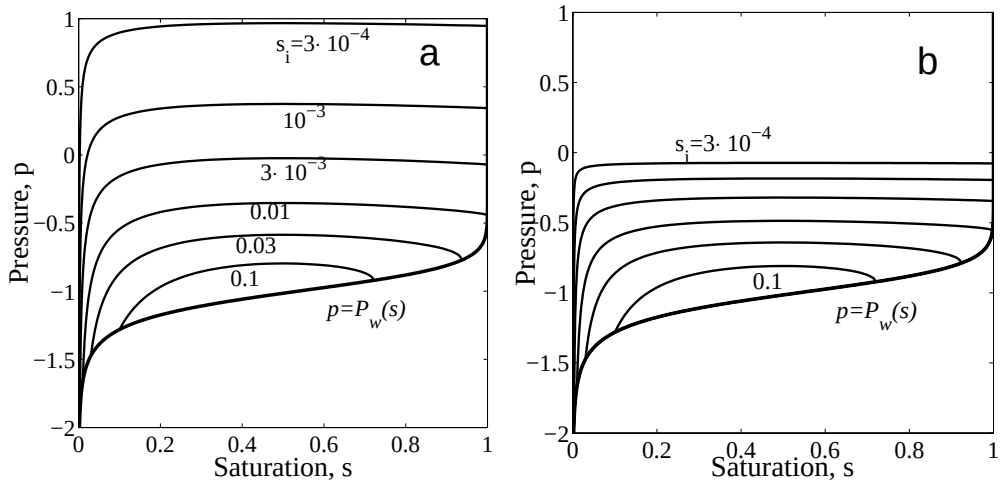

Figure 3. The typical trajectories for wetting stage of the traveling wave propagation without (a) and with (b) p-dependence of relaxation coefficient for different s_i: $\tau_s \equiv 0.5$, $p_0 = 0$, saturation behind the front is equal to 0.5 and $\gamma = 1$ for (b), while $\gamma = 0$ for (a).

Here $s_{i,j} = s(x_i, z_j, t^n)$, $\check{s}_{i,j} = s(x_i, z_j, t^{n-1})$, Δt is the current time step size, $\hbar_{x,i} = 0.5(h_{x,i-1} + h_{x,i})$, $Z_{i,j} = z_j$, and

$$k_{i\pm1/2,j}(s) = \sqrt{k(s_{i,j})k(s_{i\pm1,j})}, \qquad k_{i,j\pm1/2}(s) = \sqrt{k(s_{i,j})k(s_{i,j\pm1})}$$

At the boundary mesh points, the discrete approximation of the boundary conditions corresponding to (8) must be added to the set of discrete equations.

Finally, all of these equations may be written in matrix form on the fixed time level using lexicographical ordering of the grid points as

$$\frac{s - \check{s}}{\Delta t} + A(s)H = 0, \quad p = H + Z \tag{10}$$

$$\tau(p,s)\frac{\Pi - \check{\Pi}}{\Delta t} = p - \Pi, \quad s = S_t(\Pi) \tag{11}$$

where s, p, and H are the unknown vectors of nodal values of saturation, pressure, and total head fields respectively, A is the symmetric 5-diagonal matrix with coefficients dependent on s, and $\tau(p,s)$ is a diagonal matrix.

We solve nonlinear algebraic equations (10) and (11) by the following iteration procedure ($k+1$ indicates current iteration level):

1) let $k = 0$, and pose $p^k = \check{p}$, $s^k = \check{s}$, $H^k = \check{p} - Z$;

2) find s^{k+1} from the explicit relations

$$\tau(p^k, s^k)\frac{\Pi^{k+1} - \check{\Pi}}{\Delta t} = p^k - \Pi^{k+1}, \quad s^{k+1} = S_t(\Pi^{k+1})$$

3) solve the linear system of algebraic equations

$$A(s^{k+1})H^{k+1} + D^{k+1}H^{k+1} = D^{k+1}H^k - \frac{s^{k+1} - \check{s}}{\Delta t} \tag{12}$$

and pose $p^{k+1} = H^{k+1} + Z$. Here the diagonal matrix D^{k+1} is the approximation of the derivative of the vector valued function $(s - \check{s})/\Delta t$ with respect to p:

$$D^{k+1} = \frac{S_t'(\Pi^{k+1})}{\Delta t} \frac{d}{dp} \left(\frac{p\Delta t + \tau(p, s^{k+1})\check{\Pi}}{\tau(p, s^{k+1}) + \Delta t} \right) \Big|_{p=p^k}$$

4) set $k = k + 1$, and go to step 2). Repeat the loop until convergence is reached.

To obtain the solution for H^{k+1} we invert the matrix of the system (12) using two methods. For moderate grids ($\lesssim 5000$ nodes) we use a preconditioned conjugate gradient method based on modified incomplete Cholesky factorization, while a multigrid method (V-cycle) is used for larger grids. We note that the resulting matrix $A(s^{k+1}) + D^{k+1}$ of the system has good algebraic properties: it is symmetric, 5-diagonal, and positive definite.

Within the iteration loop 1)-4) the hysteretic state at a particular grid point is not changed, but instead iteration continues until absolute and relative errors in pressure and saturation between two consecutive iterations is less than a value ε. The change in hysteretic state is checked after convergence. To assess whether any saturation reversals have occurred at the end of each time step, we check for changes in the nodal saturations from the previous time step. If the sign of $s_{i,j} - \check{s}_{i,j}$ at a node (i, j) has changed, and $|s_{i,j} - \check{s}_{i,j}| > 10\varepsilon$, the hysteretic state for the node is changed.

4. Results of simulations

In this section we apply the numerical method to model (i) propagation of a single finger, and (ii) breakup of an initially uniform but slightly perturbed flow into fingers. In both cases, simulations were made for different values of input parameters. We noticed that a sharp-front regime may occur for some range of the input parameters (i.e. very dry soils), and very fine grids are required to adequately simulate a steep change in saturation over the front. The input parameters used in the calculations for the present results were taken within a range that allows us to deal with reasonable grids (less than 50000 nodes) for a good front approximation (the front is covered by at least four nodes). For all runs qualitatively similar behavior of the solutions were found. Therefore, we present our results only for one case with $\tau_s^0 = 5$, $\gamma = 1$, $s_i = 0.075$, $\varepsilon = 10^{-7}$, and hydraulic properties of the coarse porous medium defined in Section 2.

The single finger generation is initiated by infiltration over the finite length L at the upper boundary with the flux $q_0 > 0$. The applied flux at the soil surface shown in Figure 2 is less than the saturated hydraulic conductivity so that $q_0 < 1$. At a short time after the infiltration starts, a clearly defined single finger forms and then persistently migrates downward (Figure 4). The finger shape is determined by the total flux $Q = q_0 L$. The morphology of the finger is defined by three distinct features: finger tip with a higher water saturation, stationary finger core and a distribution layer [14]. Once developed the distribution layer remains steady while the finger tip moves at a constant velocity without change in shape and the finger core length grows at a steady rate. This scenario is fully consistent with the physical picture of the process presented in [4, 5]. The lateral spreading of the finger core is halted by the pressure inside the finger being smaller than the background pressure (Figure 4). We emphasize that the main characteristics of the finger are uniquely designated by Q, with finger velocity, finger width, and saturation at

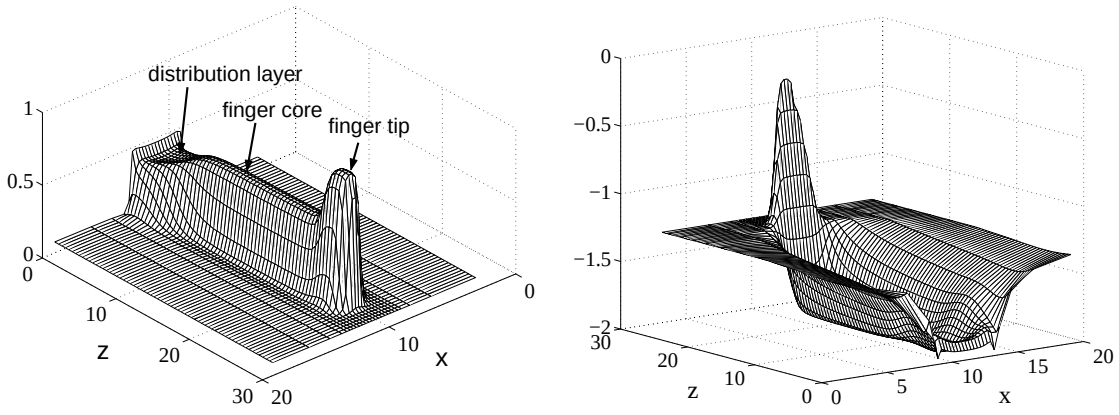

Figure 4. Saturation (left) and pressure (right) fields for the case of a single finger.

both the finger tip and the finger core increasing with Q.

The process of the breakup of the initially uniform flow into a structured system of growing perturbations is simulated in the same way as the case of the single finger propagation. In this case, however, the water is supplied along the entire top boundary, and the infiltration flux q_0 is disturbed by a high-frequency low-amplitude ($\delta \sim 10^{-2}$) perturbation. A result typical of those found for the various simulations performed is presented in Figure 5. The simulations demonstrate that:

(i) soon after flow initiation the initially uniform flow crests at the wetting front and disintegrates to a predominant perturbation wavelength, forming a set of persistent independently propagating fingers;

(ii) the water flow redistributes among fingers in the distribution region. This feature was observed experimentally by Ritsema et al. [14]. The chain of pressure 'hills' represents a border between the distribution layer and the finger cores;

(iii) the observed distance between fingers is in good agreement with the fastest growing perturbation wavelength calculated by a stability analysis of the traveling wave solution in [1] for the RRE model.

5. Discussion

The results presented in this paper demonstrate that the process of fingering can be simulated by incorporating simultaneously both the dynamic (relaxation) and the static (hysteresis) memory effects. The relaxation mechanism generates fingers [1] while hysteresis leads to their persistence. Other mechanisms for finger generation may exist, but these still need to be postulated and examined.

The simulations presented above were for initially moist porous media. Similar results also appear if the porous medium is initially very dry. Most laboratory experiments to date have imposed initially dry conditions to generate finger flow. Perhaps the relaxation mechanism is only significant for infiltration processes when the soil is initially dry enough, and this might be why finger flow has not been observed for initially moist porous

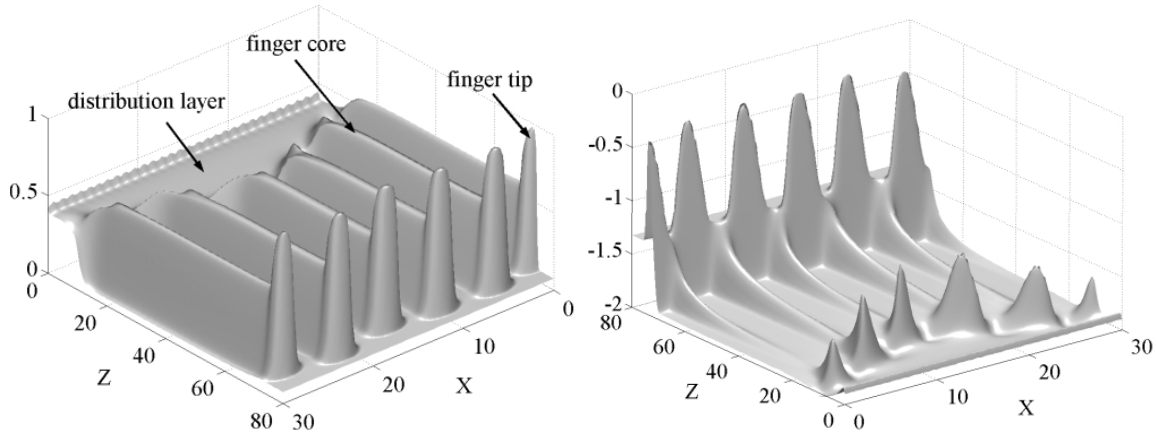

Figure 5. Saturation (left) and pressure (right) fields for the case of multiple fingers.

media. These experimental findings do not change the conclusions of the present modeling exercise. They simply point to the fact that the relaxation coefficient needs to be quantified by experiments before drawing final conclusions about the influence of initial moisture content.

Additional work is needed to improve the numerical methods to solve the governing equations (1) and (7), especially for the case of initially dry media where extremely sharp wetting fronts are involved. Adaptive grid and mesh refinement technique are appropriate to address this issue. Techniques related to variable switching might also offer some unique advantages for solving the case of initially dry porous media.

REFERENCES

1. A. G. Egorov, R. Z. Dautov, J. L. Nieber and A. Y. Sheshukov, Proc. 14th Int. Conf. on Comp. Meth. in Wat. Resour. (Delft, The Netherlands) this issue (2002).
2. J. S. Selker, J.-Y. Parlange and T. Steenhuis, Water Resour. Res. 28 (1992) 2523.
3. S. M. Hassanizadeh and W. G. Gray, Water Resour. Res. 29 (1993) 3389.
4. R. J. Glass, T. S. Steenhuis and J.-Y. Parlange, Soil Sci. 148 (1989) 60.
5. J. L. Nieber, Geoderma 70 (1996) 207.
6. A. Y. Beliaev and S. M. Hassanizadeh, Transp. Porous Med. 43 (2001) 487.
7. D. R. Nielson, G. Biggar and G. Davidson, Soil Sci. Soc. Am. Proc. 26 (1962) 107.
8. G. C. Topp, A. Klute and D. B. Peters, Soil Sci. Soc. Am. Proc. 31 (1967) 207.
9. D. E. Smiles, G. Vachaud and M. Vauclin, Soil Sci. Soc. Am. Proc. 35 (1971) 535.
10. Y. Mualem, Water Resour. Res. 10 (1974) 514.
11. M. T. Van Genuchten, Soil Sci. Soc. Am. J. 44 (1980) 892.
12. R. S. Baker and D. Hillel, Soil Sci. Soc. Am. J. 54 (1990) 20.
13. M. Panfilov, In: Recent Adv. Prob. Flow Transp. Porous Media, J. M. Crolet and M. E. Hatri (eds.) (1998) 195.
14. C. J. Ritsema, L. W. Dekker, J. M. H. Hendrickx and W. Hamminga, Water Resour. Res. 29 (1993) 2183.